



PAPER • OPEN ACCESS

## Theoretical and experimental study of nanoporous silicon photonic microcavity optical sensor devices

To cite this article: P N Patel *et al* 2012 *Adv. Nat. Sci: Nanosci. Nanotechnol.* **3** 035016

View the [article online](#) for updates and enhancements.

You may also like

- [An Improved Miniature Direct Formic Acid Fuel Cell Based on Nanoporous Silicon for Portable Power Generation](#)  
Kuan-Lun Chu, Mark A. Shannon and Richard I. Masel
- [Measurement of Tortuosity and Porosity of Porous Battery Electrodes](#)  
Tyler DuBeshter, Puneet K. Sinha, Alex Sakars et al.
- [Influence of surface roughness and interfacial layer on the infrared spectra of V-CVD grown 3C-SiC/Si \(1 0 0\) epilayers](#)  
Devki N Talwar, Zhe Chuan Feng, Chee Wee Liu et al.

# Theoretical and experimental study of nanoporous silicon photonic microcavity optical sensor devices

P N Patel<sup>1</sup>, Vivekanand Mishra<sup>1</sup> and A K Panchal<sup>2</sup>

<sup>1</sup> Electronics Engineering Department, SV National Institute of Technology, Surat-395007, Gujarat, India

<sup>2</sup> Electrical Engineering Department, SV National Institute of Technology, Surat-395007, Gujarat, India

E-mail: [vive@eced.svnit.ac.in](mailto:vive@eced.svnit.ac.in)

Received 9 April 2012

Accepted for publication 28 June 2012

Published 2 August 2012

Online at [stacks.iop.org/ANSN/3/035016](http://stacks.iop.org/ANSN/3/035016)

## Abstract

This paper reports the theoretical and experimental study of one-dimensional (1D) multilayer nanoporous silicon (NPS) photonic band gap (PBG) microcavity (MC) structures for optical sensor device applications. A theoretical framework to model the reflectance spectra relying on the Bruggeman's effective medium approximation (BEMA) and the transfer matrix method (TMM) was established for the 1D nanoporous silicon microcavity (1D-NPSMC) optical sensor device structures. Based on the theoretical background, 1D-NPSMC sensor device structures were fabricated using electrochemical dissolution of silicon wafer in hydrofluoric (HF) acid. The refractive index of the 1D-NPSMC structures was tuned by changing current density and the thickness was tuned by changing the etching time. Wavelength shifts ( $\Delta\lambda$ ) in the measured reflectance spectra were analyzed for the detection of the analyte in the porous structure. The sensing device performance was tested by different organic solvents, which showed good linear relation between the refractive index of analyte inside the pores and the wavelength shift. The application of proposed structures can be extended for the optical sensing of chemicals, gas, environmental pollutants, pathogens etc.

**Keywords:** porous silicon, photonic microcavity, transfer matrix method, Bruggeman's effective medium approximation, optical sensor device

**Classification numbers:** 4.05, 5.18, 6.03, 6.08

## 1. Introduction

Selective and accurate sensing of different chemical, biochemical and biological analytes is one of today's prime needs. At the present time, nanotechnology is helpful for the rapid and selective detection of any analyte with nanomaterials. Nanotechnology includes the design, synthesis, characterization, and applications of materials and structures whose smallest functional organization is on the nanometre scale. Photonic band gap (PBG) structures are periodic dielectric structures that control the propagation of electromagnetic wave through photonic crystals [1–3]. In past years, one-dimensional photonic band gap (1D-PBG) structures attracted a lot of attention from scientists and researchers, due to their enormous advantages and applications in optoelectronic devices,

instrumentation and sensors. In recent years, nanoporous silicon (NPS) has emerged as a promising 1D-PBG structure in nanoscale optical sensor devices due to tremendous advantages [4]. Its large surface area within a small volume, easy fabrication, controllable pore sizes, convenient surface chemistry and ability to modulate its refractive index as a function of depth [5] makes it suitable for many applications. One-dimensional nanoporous silicon microcavity (1D-NPSMC) is realized by two Bragg mirrors and a defect layer that breaks the periodicity of the refractive index profile [6]. The sharp photonic resonance dip in the reflectance spectra of 1D-NPSMC makes it suitable for the accurate optical sensing applications. In the nanoporous structure, 1D-NPSMC consists of a large number of pores which are used as the hosts for the detection of gas, chemical, biochemical and bioanalytes, because its optical properties [7]



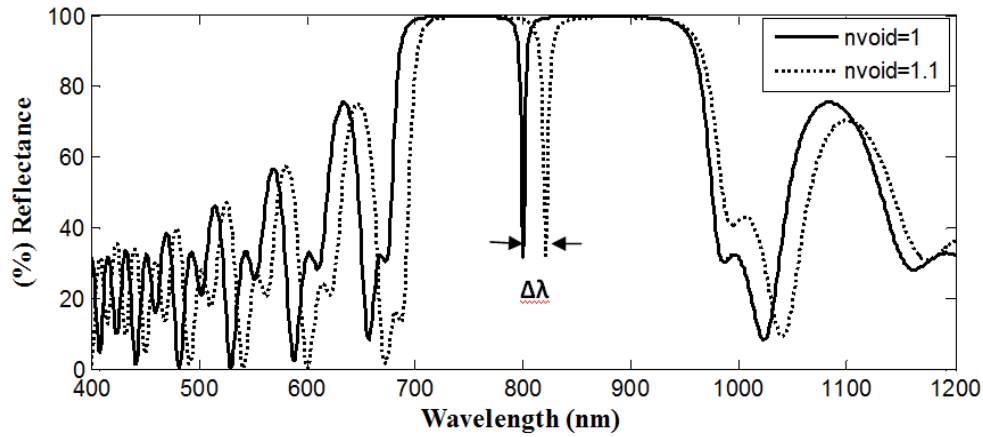


Figure 1. Reflectance spectra of 1D-NPSMC structures.

are highly sensitive to the presence of chemical and biological species inside the pores. All these features make NPS structures suitable for many emerging optical devices and sensor applications [8–12].

The objective of this work is numerical modelling and fabrication of multilayered photonic microcavity (MC) structures using NPS for optical sensor device applications. In section 2, the theory related to modelling based on the Bruggeman’s effective medium approximation (BEMA) and transfer matrix method (TMM) has been set up for the 1D-NPSMC structures in order to predict their optical reflectance. In section 3, the experimental detail for the fabrication of multilayered MC structures is presented. In section 4, theoretical and experimental study of 1D-NPSMC is done and the results are compared. Finally, testing of the sensor device by analyzing and comparing the wavelength shifts ( $\Delta\lambda$ ) in the reflectance spectra of different organic solvents such as methanol, ethanol, propanol and benzene is performed.

## 2. Theory

NPS is a two phase composite, being a mixture of air and the silicon solid phase containing the silicon network with silicon walls and nanopores. The sponge-like structure of NPS makes it a suitable material for optical devices and sensor applications. According to optics theory, the reflectance spectrum of 1D-NPSMC structure is governed by the interferometric Fabry–Perot relationship [13]. Light reflected from the top interface (air-NPS) constructively interferes with light from the bottom interface (NPS-Si substrate) of the 1D-NPSMC structure, and forms the typical Fabry-Perot fringes in the reflectance spectrum [14]. The fringe pattern is closely related to effective optical thickness, which is a product of physical thickness  $h$  and refractive index  $n$  of the structure, by the relationship

$$m\lambda = 2nh, \tag{1}$$

where  $m$  is an integer (the spectral peak order) and  $\lambda$  is the peak wavelength.

For bare (without any analyte) 1D-NPSPBG structure ( $n_{\text{void}} = 1.0$ ), the refractive index of the structure is  $n$ . When

the pores of the 1D-NPSMC structure are filled with an analyte (e.g. gas, chemical, bio-chemical and bioanalytes), the overall effective refractive index of the structure increases from  $n$  to  $n + \Delta n$  with shift in wavelength from  $\lambda$  to  $\lambda + \Delta\lambda$  in the reflectance spectra as shown in figure 1, due to increased overall optical thickness of the structure. By analyzing the wavelength shift ( $\Delta\lambda$ ) in the reflectance spectra for different refractive index values, the capture of the analyte in the structure can be detected.

BEMA [15] and the TMM [16] theory are used as the base of the modelling for the analysis of the wavelength shift in the reflectance spectra of the structures. Refractive index  $n$ , thickness  $h$  and porosity  $P$  of the layers are the key parameters and the base of the numerical modelling. Layer refractive index is related with the porosity by BEMA model as described by following equation

$$(1 - P) \frac{n_{\text{Si}}^2 - n_{\text{nps}}^2}{n_{\text{Si}}^2 + 2n_{\text{nps}}^2} + P \frac{n_{\text{void}}^2 - n_{\text{nps}}^2}{n_{\text{void}}^2 + 2n_{\text{nps}}^2} = 0, \tag{2}$$

where  $P$  is porosity of the NPS,  $n_{\text{Si}}$  the refractive index of silicon,  $n_{\text{nps}}$  the refractive index of NPS,  $n_{\text{void}}$  the refractive index of the medium inside the pores (air/analyte). This approximation is acceptable because the size of the pores is much smaller than the wavelengths of incidence light in the near ultraviolet-visible-infrared (UV-Vis-IR) region. In this range, the electromagnetic radiation does not distinguish between silicon and void, and it is possible to treat the NPS as a homogeneous medium.

Theoretical study of wave transmission in a 1D-NPSPBG structure is based on TMM. 1D-NPSPBG structures consisting of alternating PS layers of different refractive indices coupled to a homogeneous medium characterized by refractive indices  $n_0$  at the initial medium and  $n_s$  at final medium are considered. A general schematic diagram of 1D-NPSPBG structure is shown in figure 2. In figure 2,  $A(x)$  and  $B(x)$  represent the amplitudes of right and left travelling waves, respectively,  $n_1$  and  $n_2$  are the layer refractive indices,  $h_1$  and  $h_2$  are the thicknesses of the respective layers and  $\Lambda$  is the period of the structure ( $\Lambda = h_1 + h_2$ ).

An electromagnetic field produces a characteristic matrix at each interface. The electric field of a general plane wave solution can be written as  $E = E(x)e^{i(\omega t - \beta z)}$  and its

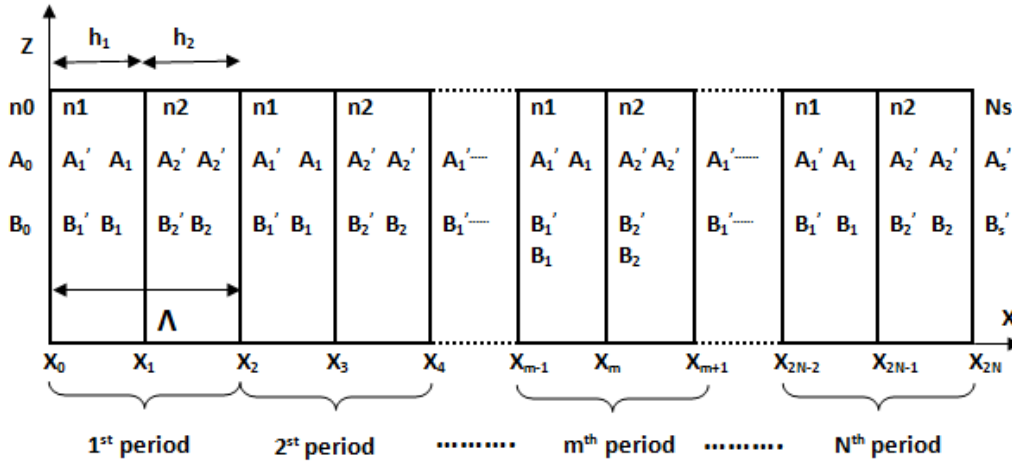


Figure 2. Schematic diagram of 1D-NPSPBG structure.

distribution can be written as

$$E(x) = \begin{cases} A_0 e^{-ik_{0x}(x-x_0)} + B_0 e^{ik_{0x}(x-x_0)}, & x < x_0, \\ A_m e^{-ik_{mx}(x-x_m)} + B_m e^{ik_{mx}(x-x_m)}, & x_{m-1} < x_0 < x_m, \\ A_s e^{-ik_{sx}(x-x_0)} + B_s e^{ik_{sx}(x-x_{2N})}, & x_{2N} < x, \end{cases} \quad (3)$$

where  $k_{mx}$  is the  $x$  component of the wave vectors  $k_{mx} = \omega n_m \cos \theta_m / c$  and  $\theta_m$  is the ray angle in each layer.  $A_m$  and  $B_m$  represent the amplitudes of the plane wave at the interface  $x = x_m$ .

If the two general amplitudes of  $E(x)$  are represented as column vectors, the plane waves at different layers can be related by

$$\begin{bmatrix} A_{m-1} \\ B_{m-1} \end{bmatrix} = D_{m-1}^{-1} D_m \begin{bmatrix} A'_m \\ B'_m \end{bmatrix} = D_{m-1}^{-1} D_m P_m \begin{bmatrix} A_m \\ B_m \end{bmatrix}, \quad m = 1, 2, \dots, 2N + 1, \quad (4)$$

where matrices  $D_m$  are the dynamical matrices given by

$$D_m = \begin{cases} \begin{pmatrix} 1 & 1 \\ n_m \cos \theta_m & -n_m \cos \theta_m \end{pmatrix}, & \text{for TE wave,} \\ \begin{pmatrix} \cos \theta_m & \cos \theta_m \\ n_m & -n_m \end{pmatrix}, & \text{for TM wave,} \end{cases} \quad (5.1)$$

and  $P_m$  is the propagation matrix that can also be written as

$$P_m = \begin{pmatrix} e^{ik_{mx}h_m} & 0 \\ 0 & e^{-ik_{mx}h_m} \end{pmatrix}. \quad (5.2)$$

If equation (4) is solved with different values of  $m$ , the relation between  $A_0, B_0$  and  $A'_s, B'_s$  can be written as

$$\begin{pmatrix} A_0 \\ B_0 \end{pmatrix} = D_0^{-1} [D_1 P_1 D_1^{-1} D_2 P_2 D_2^{-1}]^N D_s \begin{pmatrix} A'_s \\ B'_s \end{pmatrix} = \begin{bmatrix} M_{11} & M_{12} \\ M_{21} & M_{22} \end{bmatrix} \begin{bmatrix} A'_s \\ B'_s \end{bmatrix}, \quad (6)$$

where  $N$  is the number of periods in the structure. From equation (6) the characteristic matrix can be written as

$$M = D_0^{-1} [D_1 P_1 D_1^{-1} D_2 P_2 D_2^{-1}]^N D_s. \quad (7)$$

The reflectance of monochromatic plane wave through the 1D-NPSPBG structures is calculated from the matrix elements. If the light is incident from medium 0, the reflectance coefficients are defined as

$$r = \begin{pmatrix} A_0 \\ B_0 \end{pmatrix}_{B_s=0}. \quad (8)$$

Using matrix equation (6) and definitions in equations (8), the following relation is obtained:

$$r = \frac{M_{21}}{M_{11}}. \quad (9)$$

Reflectance is given by equation

$$R = |r|^2 = \left| \frac{M_{21}}{M_{11}} \right|^2, \quad (10)$$

provided that medium 0 is lossless.

In order to apply the above-mentioned theory to the study of the optical sensing performance of 1D-NPSPBG structures, the above generalized model is modified for the microcavity structure shown in figure 3, and the simulation program was set up using Matlab software based on different structural and optical parameters. In figure 3,  $n_s$  is the refractive index of the substrate and  $N$  is the number of periods. The microcavity was realized by inserting a cavity layer of high current density between two identical distributed Bragg reflectors (DBR1 and DBR2) with six repetitions of a current density and etching time sequences, as shown in figure 3.

All the simulations are done for the normal incidence of the light. Refractive index of ambient medium  $n_0$  and that of substrate  $n_s$  are 1.0 and 3.6, respectively, while the wavelength range of analysis is 500–1100 nm. The critical design parameters for simulation are: porosity, refractive index and the thickness of each respective layer. The refractive index is related with porosity by BEMA (equation (2)). The refractive indices  $n_1, n_2$  and  $n_c$  are chosen as 1.70, 2.60 and

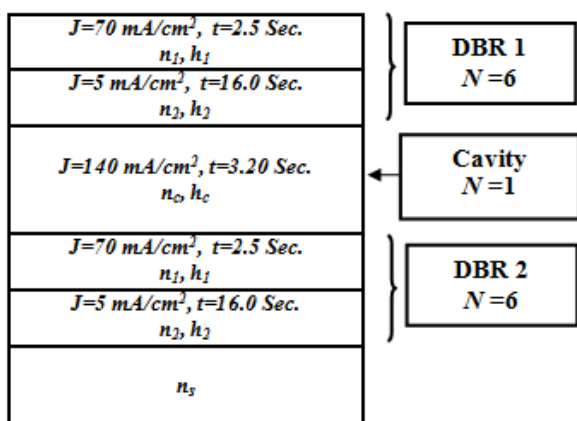


Figure 3. Schematic diagram of 1D-NPSMC structure.

1.63, which are suitable for fabrications. The thicknesses of different layers have been calculated to obtain a resonant wavelength at 750 nm by means of equations

$$\frac{\lambda_0}{4} = n_1 h_1 = n_2 h_2 \tag{11}$$

and

$$\frac{\lambda_0}{2} = n_c h_c. \tag{12}$$

### 3. Experimental

1D-NPSMC structures were fabricated by electrochemical etching of p-type Si wafer (<100>, 0.01– 0.02 Ω cm, 275 μm, 20 cm<sup>2</sup>). The schematic diagram of the electrochemical etching cell [17] is shown in figure 4.

As shown in figure 4, the base and the cap of the electrochemical etching cell were made with SS 320 metal. Silicon wafer was placed inside the base and sealed with an O-ring and exposed to the electrolyte. The electrolyte mixture was kept in the highly HF resistant polymer polytetrafluoroethylene (PTFE), which was in contact with the platinum grid, used as a cathode. First, silicon wafer was cleaned using the standard piranha cleaning method. The PTFE bath was filled with the etching solution of 40% aqueous HF and 99% ethanol, mixed in the ratio of 1 : 2. The cathode was immersed in the electrolyte solution and the distance between anode and cathode was kept about 4.5 cm. Periodic constant current square wave was applied by programmable DC power supply (PWS 4305, Tektronix). A constant current mode was used for the anodization process as it is beneficial in terms of regulation [18]. Applied current density ( $J$ ) and the etching time ( $t$ ) profile are responsible for the change in refractive index ( $n$ ) and the physical thickness ( $d$ ) profile of the layer, respectively.

After electrochemical etching, these structures were rinsed in DI water for 10 min and dried at room temperature. Structural morphology (plan and cross sectional view) was examined by field-emission gun scanning electron microscope (FEG-SEM) JSM-7600, JEOL. Testing of the sensor device was done by the measured reflectance spectra before, during and after exposure to various organic solvents using spectrometer (MayaPro-2000, Ocean Optics). All measurements were done in the air. Polished silicon wafer was used as reference in the reflectance measurements.

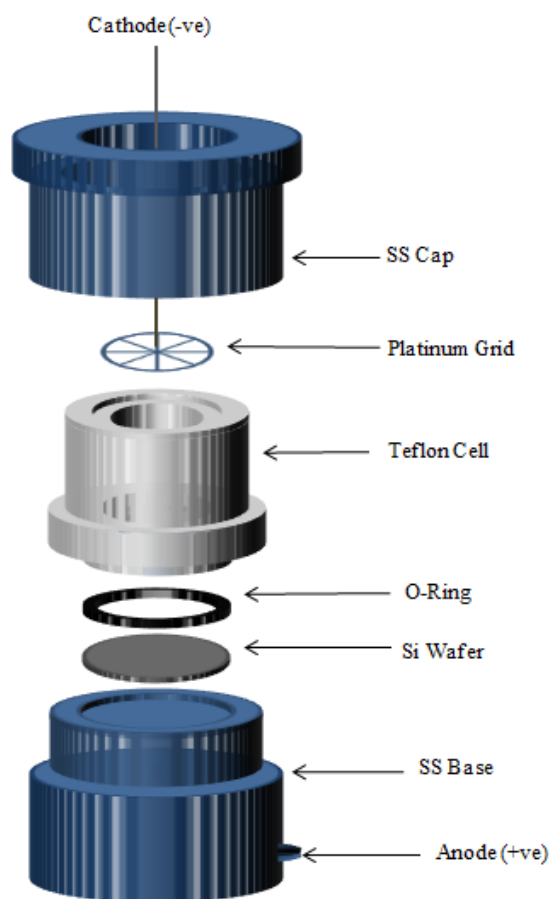


Figure 4. Electrochemical etching cell.



Figure 5. Fabricated 1D-NPSMC structure.

### 4. Results and discussion

The prepared structures show distinct green, blue and red colours distribution over the entire surface (figure 5). Porous structure in the bulk silicon is strongly responsible for the change in the surface colour due to the shifting in the bandgap energy of silicon [19].

Structural morphology (plan and cross-sectional views) was examined by SEM. Figure 6 shows the surface morphology of the structures in SEM plan view. The array of void spaces (dark) in silicon matrix (bright) can be seen clearly in the plan view SEM image. The morphology of the structure shows that the electrochemical etching is done uniformly on the surface and created the granular structure in a spherical shape. A large number of pores distributed in all

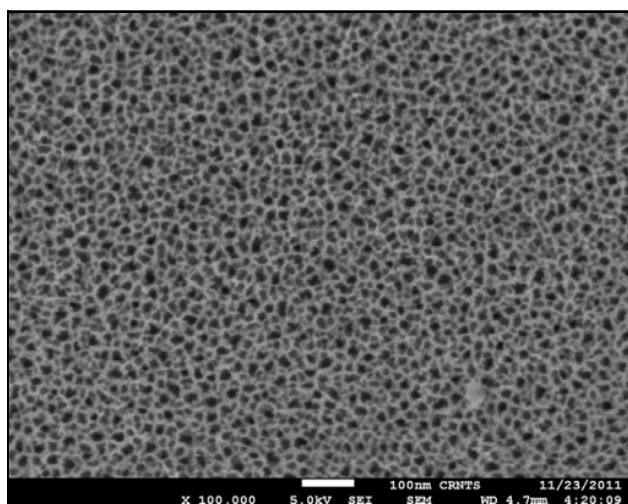


Figure 6. SEM plan view of 1D-NPSMC structure.

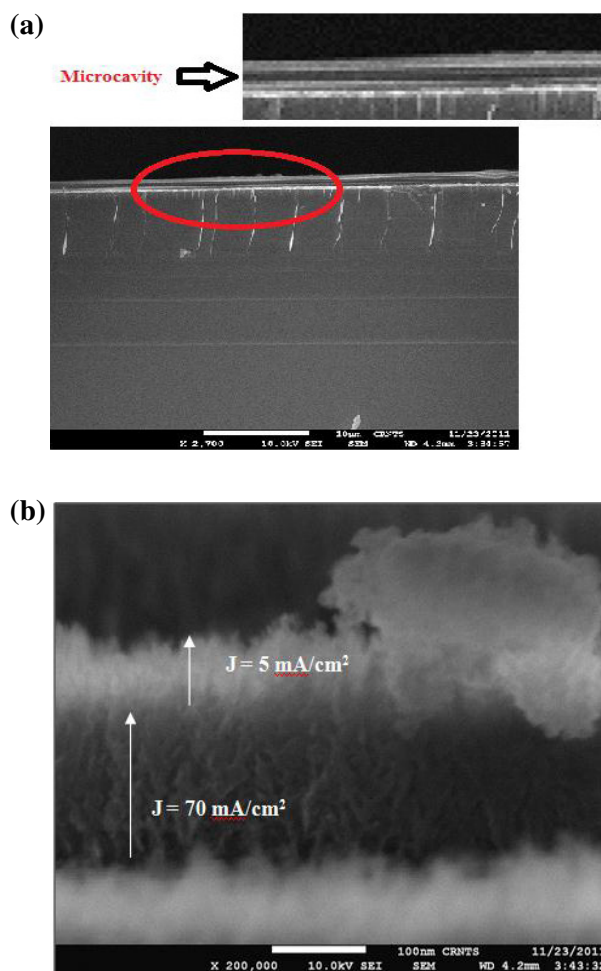


Figure 7. (a) SEM cross-sectional view of NPSMC structure; (b) low and high porosity layers of NPSMC.

directions can be observed in figure 6 with mean pore size of 24 nm measured using Image J software.

The SEM cross-sectional image of the 1D-NPSMC structure is shown in figure 7. Multilayered stacks are clearly observed in this figure. These stacks are due to the periodic variation in the refractive index profile through the current density variation for different etching times. The cavity layer

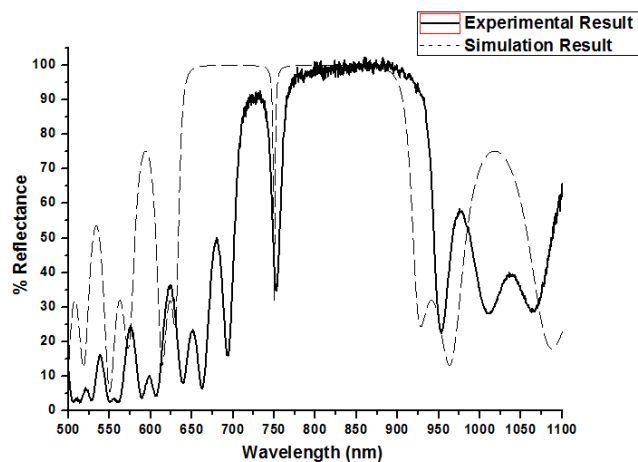


Figure 8. Simulated and measured reflectance spectra of 1D-NPSMC structure.

Table 1. Calculated and measured wavelength shift.

Organic solvent	Refractive index of solvent ( $n$ )	Simulated wavelength shift $\Delta\lambda$ (nm)	Measured wavelength shift $\Delta\lambda$ (nm)
Methanol	1.328	80.00	84.00
Ethanol	1.361	86.00	71.50
Propanol	1.385	91.00	95.00
Benzene	1.501	117.00	130.00

of the microcavity structure can be clearly observed in the inset view of figure 7(a). In figure 7(b), the light grey stripes correspond to low porosity layers ( $J = 5 \text{ mA cm}^{-2}$ , high refractive index) and the dark grey stripes correspond to the high porosity layers ( $J = 70 \text{ mA cm}^{-2}$ , low refractive index). Further, the branched cylindrical structure possessed by the pores is also clearly visible in figure 7(b) which shows that the pore growth occurs in the depth (perpendicular to the surface) of the structure.

Reflectance spectrum of simulated and fabricated 1D-NPSMC structures with the sharp photonic resonance dip centred at 750 nm can be observed in figure 8.

Some discrepancies are noticed between simulated and measured values in the reflectance spectra of figure 8 because the simulation does not take into account the fact that the top layer is in contact with HF solution during the whole electrochemical process. The anodization condition might drift as the sample thickness, the refractive index of stacks and the solution composition change with the depth because of limited exchange through the pores. This fact caused the difference of experimental results in comparison with simulation ones.

After modelling, fabrication and characterization of 1D-NPSMC structures, their performance as an optical sensor device was tested by analyzing the resonance photonic stop band shift in the reflectance spectra with the values of the refractive indices of different organic solvents in simulations and by exposure of the sensor device structure to 100% concentration of different organic solvents. Calculated and measured wavelength shifts of the reflectance spectra of organic solvents such as methanol, ethanol, propanol and benzene are listed in table 1.

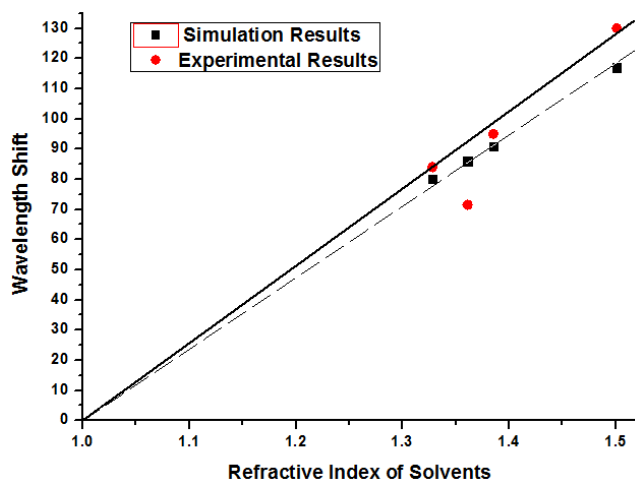


Figure 9. Refractive index versus wavelength shift.

It is clearly observed that the wavelength in the reflectance spectra of the 1D-NPSMC sensor device structure is shifted to higher wavelength because the pores were filled with organic solvent ( $n_{\text{void}} > 1.0$ ). The filled pores with organic solvent increase the overall effective refractive index of the structure and consequently increase its optical thickness. This effect promotes the wavelength shift in the reflectance spectrum. The strength of the wavelength shift depends on the refractive index of the organic solvent. The higher the refractive index of the solvent, the higher the wavelength shift that is observed.

As listed in table 1, when the sensor device structure was exposed to organic solvents of a high refractive index, large variations in the reflectance spectra were observed; correspondingly, when the structure was exposed to organic solvents of a low refractive index, small variations in the reflectance spectra were observed in both simulation and experiments. This is due to the variations in the effective refractive index of the 1D-NPSMC sensor device structure according to the refractive index of the organic solvent adsorbed in its pores. The relationship between refractive index of the organic solvent and the wavelength shift is plotted in figure 9 from the results of table 1.

Figure 9 shows the good linear fitting for the graph of the refractive index values versus wavelength shift for the simulation as well as experimental results. In figure 9 it is observed that almost all the experimental points are on the linear fitting curve except for a few points. The origin of the mismatch of a few points may be due to some type of chemical reaction of this solvent with the surface of the structure. Sensitivity is one of the most important issues to evaluate the performance of the sensor device. In this case the response of the sensor device is evaluated throughout the change of the wavelength shift ( $\Delta\lambda$ ) of the reflectance spectrum due to the change of the refractive index ( $\Delta n$ ). Sensitivity ( $S$ ) is defined as

$$S = \frac{\Delta\lambda}{\Delta n} \quad (13)$$

This parameter shows to be a good indicator for sensing measurement in the 1D-NPSMC sensing devices. Calculated and measured sensitivity are 264.27 and 265.89.

It is also observed during the experiment that after complete evaporation of each organic solvent, the reflectance spectra of the structures promptly return to their original waveform position. This implies that the change of reflectance spectra is indicative of the presence or absence of organic solvents in the nanopores, and that the change of the spectra of the 1D-NPSMC sensor device structure is temporary. These results are very useful for the development of effective reversible 1D-NPSMC based optical sensor devices.

## 5. Conclusions

To conclude, successful modelling and fabrication of nanoporous silicon photonic microcavity structures as an optical sensor device was done. A simulation program has been developed for the numerical study and design of the 1D-NPSMC structures, which was an excellent agreement with the experimental one. A large number of uniformly distributed nanosized pores were observed in the plan view of SEM characterization of the fabricated sensor device structures. A periodic multilayered structure with variation of the refractive index and thickness was observed in the cross-sectional SEM characterization. The imperfection of interfaces created by the electrochemical etching may be the cause of the deviations of the simulation and the experimental reflectance spectra. Testing of the sensor device by the simulation and the experiments for organic solvents detection showed good linear relation. Sensitivity analysis showed excellent agreement between theoretical and experimental results. It was noticed that after complete evaporation of the solvent from the nanoporous structure, the photonic resonance dip comes back to its original position, which is an excellent property of these devices for developing reversible sensing applications.

## Acknowledgments

This work was supported by the grant from Defence Research and Development Organization (DRDO), Government of India. The authors are also thankful to the Centre for Research in Nanotechnology & Science CRNTS and Sophisticated Analytical Instrumentation Facility SAIF at the Indian Institute of Technology Bombay (IIT Bombay) for the structural characterization of the samples.

## References

- [1] Yablonovitch E 1987 *Phys. Rev. Lett.* **58** 2059
- [2] Yablonovitch E 1993 *J. Opt. Soc. Am. B* **10** 283
- [3] Lipson R H and Lu C 2009 *Eur. J. Phys.* **30** 33
- [4] Canham L 1997 *Properties of Porous Silicon* 1st edn (London: INSPEC) chapter 1
- [5] Cullis A G, Canham L T and Calcott P D J 1997 *J. Appl. Phys.* **82** 909–65
- [6] Koshida N (ed) 2009 *Device Applications of Silicon Nanocrystals and Nanostructures* 1st edn (New York: Springer Science) chapter 10
- [7] Theiss W 1997 *Surf. Sci. Rep.* **29** 91
- [8] Tommasi E, De Stefano L, Rea I, Di Sarno V, Rotiroli L, Arcari P, Lamberti A, Sanges C and Rendina I 2008 *Sensors* **8** 6549

- [9] Solanki C 2007 Study of porous silicon layers transfer for applications in thin film monocrystalline silicon solar cell *PhD Thesis* Katholieke University Leuven, Belgium, chapter 2
- [10] Weiss S M and Fauchet P M 2003 *Phys. Status Solidi a* **2** 556
- [11] Saha H 2008 *Int. J. Smart Sens. Intell. Syst.* **1** 34–6
- [13] Chi Do T, Bui H., Van Nguyen T., Anh Nguyen T, Hai Nguyen T and Hoi Pham V 2011 *Adv. Nat. Sci.: Nanosci. Nanotechnol.* **2** 035001
- [13] Min H-K, Yang H-S and Cho S M 2000 *Sensors and Actuators B* **67** 199
- [14] Ouyang H and Fauchet P M 2005 *Proc. SPIE Opt. East* **6005** 600508
- [15] Khardani M 2007 *Phys. Status. Solidi. c* **4** 1986
- [16] Born M and Wolf E 1999 *Principles of Optics* 7th edn (Cambridge: Cambridge University Press) chapter 3
- [17] Patel P N, Mishra V and Panchal A K 2012 *J. Optoelectron. Biomed. Mater.* **4** 19–28
- [18] Panchal A K, Kale P G and Solanki C S 2007 Preparation of porous silicon nanostructure for solar photovoltaic applications *Proc. Int. Conf. on Advances in Energy Research ICAER 12–14 (December, 2007, Macmillan India)* p 797
- [19] Dubey R and Gautam D K 2009 *Opt. Quant. Electron.* **41** 189